

Identification and Control of Rotating Disk Vibration

C. J. Radcliffe

Department of Mechanical Engineering,
Michigan State University,
East Lansing, Mich. 48824

C. D. Mote, Jr.

Department of Mechanical Engineering,
University of California,
Berkeley, Calif. 94720

Small amplitude, transverse vibration of a circular disk can be viewed as a superposition of travelling waves each wave corresponding to a particular vibration mode. When the plate damping is small, the transverse motion of the plate is often dominated by response in one mode [1]. The active control method discussed here used an on-line FFT analysis of the rotating disk displacement to periodically identify the dominant mode of the disk response in a changing operating environment. Active control forces were applied electromagnetically to the disk to suppress the amplitude of that particular mode. In laboratory tests, the prototype controller reduced the modal amplitude to less than 15 percent of the uncontrolled value. Analytical predictions correlated well with these laboratory observations.

Introduction

Centrally-clamped rotating disks are the basic machine element of steam and gas turbines, grinding wheels, circular saws, and computer disk memories. Large amplitude transverse vibration of rotating disks can cause failure of turbine wheels due to wheel-to-case contact, cutting inaccuracy for grinding wheels and circular saws and head tracking errors in computer disk memories.

The research in transverse vibration control reported herein was motivated by the economic advantage to the wood industry of cutting with thin, stable circular saws. Cutting residual resulting from a combination of saw blade transverse vibration and tooth kerf accounts for more than 20 percent of wood volume. The economic and natural resource loss on a national or worldwide basis is enormous. Active control of transverse vibration can reduce cutting residual by decreasing both the vibration amplitude and the minimum saw blade thickness required for stable operation. Although focussed on circular saws, the control method discussed here has wider applications in rotating machinery.

Rotating disk vibration, though representable by an infinite number of vibration modes, is usually dominated by the response of a limited number of modes when disk damping is small and excitation is over a limited frequency band. A stability theory has been developed for circular saws which assumes disk vibration to be dominated by response of a single mode. This stability theory has been confirmed by measurements in a production environment [1] which showed a direct correspondence existed between total vibration amplitude and the proximity of disk rotation speed to a rotation speed where a constant, stationary traverse force resonates a single mode of the disk.

The problem addressed is the active control of thin, axisymmetric rotating disks with small internal damping using external transverse control forces. Ellis and Mote [2]

developed a control system which generated a transverse force in response to measured transverse displacement and velocity of the disk. This system controlled low frequency vibration ($< 50\text{Hz}$), but excited higher frequency instability above the bandwidth of their control system ($> 8\text{kHz}$). The resultant instability limited the effectiveness of the control system through saturation of the electromagnets used to generate control forces. Balas, et al. [3] reported a similar instability when modal control was employed on large scale structures with small damping. High frequency errors contaminating the observed modal amplitudes, termed "observation spillover," when amplified by the control system, excited this instability by "control spillover." Controller stability was increased through low-pass filtering of the observation signal [2, 3]. However, phase shifts in the filters resulted in eventual instability of the control systems [2].

Guaranteeing stability of distributed parameter control systems is inherently more difficult than for lumped parameter control systems. When controlling a finite number of modes in a distributed structure, the central stability problem is the isolation of the control system action from modes not under control. This isolation is accomplished through elimination of either "observation spillover" or "control spillover." That is, stability of uncontrolled modes is assured when they are either not detected by the control system or not excited by the control. The elimination of spillover prevents control system excitation of the uncontrolled modes.

Control spillover can be prevented by developing a control force distribution equivalent to the generalized force distribution of the mode under control. Such a control force cannot excite other modes. However, when a finite number of discrete control forces are used to suppress the single mode, orthogonality with all other modes is not possible, and "control spillover" always results. Control spillover can be reduced by increasing the number of control forces, and hence the accuracy of the force distribution, and by ensuring the control force only oscillates at the characteristic frequency of the mode under control.

Contributed by the Dynamic Systems and Control Division for publication in the JOURNAL OF DYNAMIC SYSTEMS, MEASUREMENT, AND CONTROL. Manuscript received by the Dynamic Systems and Control Division, May 18, 1982.

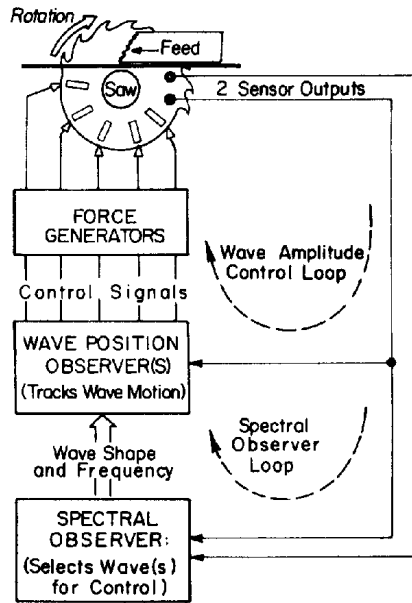


Fig. 1 Spectral control structure

Active Vibration Control Using Spectral Analysis

The application of spectral analysis to the active vibration control of rotating disks was investigated. The spectral observer loop shown in Fig. 1 identified the vibration modes of dominant amplitude and selected one mode for control. Control forces to suppress that mode were developed by the amplitude control loop also shown in Fig. 1.

Modal distributions in a rotating axisymmetric disk are represented by pairs of waves propagating in opposite directions around the disk. The "forward travelling" wave propagates in the direction of disk rotation and the "backward travelling" wave propagates in the opposite direction [4, 5]. The characteristic frequencies corresponding to the forward travelling waves, as seen by the nonrotating observer, are increased by disk rotation. Similarly the characteristic frequencies corresponding to the backward travelling waves are reduced by rotation. The lowest characteristic frequency seen by a nonrotating observer always corresponds to a backward travelling wave.

Nomenclature

a = inner radius
 $A_{mn}(r)$ = amplitude of wave (m, n)
 b = peripheral radius
 c_s, c_r = stationary and rotating damping coefficients
 $C_{mn}(t), D_{mn}(t)$ = disk generalized displacement coordinates
 m = number of nodal circles
 n = number of nodal diameters
 $q(r, \theta, t)$ = nonconservative transverse load
 $q_s(r, \theta, t), q_r(r, \theta, t)$ = stationary and rotating damping forces
 $R_{mn}(r)$ = radial distribution of mode (m, n)
 $u_{mn}(r, \theta)$ = modal distribution of mode (m, n)
 v_{mn} = rotation velocity of mode (m, n)
 $V_{mn}(r, \theta, t)$ = predicted transverse velocity of mode (m, n)

The wave form in circular plate vibration can be represented by

$$u_{mn}(r, \theta) = A_{mn}(r) \sin(n\theta) \quad (1)$$

where the radial function, $A_{mn}(r)$, is a linear combination of Bessel functions. The forms are identified by integer numbers of nodal circles, m , and nodal diameters, n . On a rotating disk, the transverse displacement, $y_{mn}(r, \theta, t)$ of a single backward travelling wave, viewed in a nonrotating reference frame, becomes [5]:

$$y_{mn}(r, \theta, t) = A_{mn}(r) \sin\{n(\theta - \phi_{mn}) + (\omega_{mn})t\} \quad (2)$$

Here, the disk rotates in a positive coordinate direction. Forward travelling waves are represented by (2) with "n" replaced by "-n."

Spectral analysis was employed to identify the single backward travelling wave for control from the total transverse response of a rotating disk. A Fourier transform of the measured displacement yields the amplitude and phase spectra, $A(\omega)$ and $\delta(\omega)$. Local maxima in $A(\omega)$ locate the characteristic frequencies. At each characteristic frequency, the number of nodal diameters, n , defining the wave form and wave propagation direction can be determined through two phase spectra, $\delta_i(\omega)$ where $i = 1, 2$. These spectra were computed from two displacements recorded simultaneously at sensor locations (r, θ_i) with $i = 1, 2$.

The phase spectrum is given by the phase in (2). At ω_{mn} for sensor location (r, θ_i) ,

$$\delta_i(\omega_{mn}) = n(\theta_i - \phi_{mn}) \quad (3)$$

The relationship (3), evaluated at the two sensor positions, (r, θ_i) can be used to compute the number of nodal diameters, n ,

$$n = [\delta_1(\omega_{mn}) - \delta_2(\omega_{mn})] / [\theta_1 - \theta_2] \quad (4)$$

Positive "n" in (4) denotes a backward travelling wave and negative "n" denotes a forward travelling wave.

Modes with one or more nodal circles have not been observed to contribute significantly to disk vibration, and accordingly they have never been candidates for control in these rotating disk problems. The number of nodal circles, m , defining a mode can be determined from the amplitude spectrum $A_j(\omega_{mn})$ by positioning the sensors at different radii, r_j . Nodal circle modes with $m \geq 1$ were not identified herein.

Once A_{mn} , n , and ω_{mn} , are determined, individual waves were selected for control. Here, the lowest frequency wave with amplitude greater than 75 percent of the maximum spectral amplitude was selected for control. This criterion was

$y(r, \theta, t)$ = transverse displacement
 $y_{mn}(r, \theta, t)$ = transverse displacement of mode (m, n)
 $\hat{y}_{mn}(r, \theta, t)$ = approximate transverse displacement of mode (m, n)
 $Y_{mn}(r, \theta, t)$ = predicted transverse displacement of mode (m, n)
 δ = phase angle
 ζ = damping ratio
 θ = angular coordinate
 ϕ_{mn} = initial angular position of mode (m, n)
 ω = angular frequency
 ω_{mn} = characteristic frequency of mode (m, n)
 Ω = disk rotation frequency
 $\tau = 2\pi/\omega$ = filter recirculation time (period)

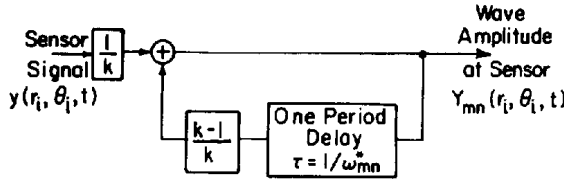


Fig. 2 Comb filter used to observe wave motion in laboratory tests

chosen because of the observed importance of low frequency waves to the disk response [1].

The separation (Fig. 1) of the spectral observer from the control force generation was required by the time necessary to compute a Fast Fourier Transform (i.e., approx. 30 seconds on a PDP 8/E minicomputer). This time delay was too long to allow on-line control of the disk using only the results of the spectral analysis. Instead, a wave amplitude control loop tracked the position of the wave selected for control and then applied the control forces. Extension to the control of multiple waves can be accomplished by superposition of control forces developed for each wave.

The wave position observer in the wave amplitude control loop measures the displacement of a single wave by filtering the total disk transverse displacement. A first order, recursive, digital, "comb filter" [6] was selected for this purpose because of its simplicity (Fig. 2). The filter frequency was set equal to the wave characteristic frequency as determined by the spectral observer. The filtered signal is recirculated at the characteristic frequency, with the weighing constant $k > 1$; see Fig. 2. Frequency components of the disk displacement at the recirculation frequency and its harmonics are passed by the filter while other components are not. The prediction of wave displacement, Y_{mn} , from the measured disk displacement after filtering is

$$Y_{mn}(r, \theta, t) = (1/k) \sum_{i=0}^{\infty} \{ [(k-1)/k] y(r, \theta, t - i\tau) \} \quad (6)$$

where: $\tau = 2\pi/\omega_{mn}$, recirculation time

The maximum attenuation of this filter for signals with periods different from the recirculation interval is $1/(2k-1)$. The filter selectivity is improved by increasing k . However, increasing k also decreases the speed of response of the filter. A reasonable compromise was found to be $k=8$ and this value was used for all analyses and laboratory tests.

The angular propagation velocity, v_{mn} , of a wave can be calculated from its characteristic frequency [5].

$$v_{mn} = \omega_{mn}/n \quad (7)$$

From measured $Y_{mn}(r, \theta, t)$ and v_{mn} , a predicted $Y_{mn}(r_i, \theta, t)$ for all θ is obtained by delaying $Y_{mn}(r_i, \theta_i, t)$ by the time required for the mode to propagate from θ_i to θ .

$$Y_{mn}(r_i, \theta, t) = Y_{mn}(r_i, \theta_i, t - T) = (1/k) \sum_{i=0}^{\infty} \{ [(k-1)/k] y(r_i, \theta_i, t - i\tau - T) \} \quad (8)$$

where: $T = (\theta - \theta_i)/v_{mn}$, propagation time

The predicted wave displacement at any θ is given by the amplitude of the signal in the comb filter's serial delay element at a point corresponding to the propagation time, T . In addition, the wave transverse velocity, dY_{mn}/dt , can be predicted from the recirculated signal in the delay element at a point corresponding to a quarter period phase lead from the wave displacement;

$$V_{mn}(r_i, \theta, t) = Y_{mn}(r_i, \theta, t + (\tau/4)) = (1/\omega_{mn}) d[Y_{mn}(r_i, \theta, t)]/dt \quad (9)$$

The wave amplitude controller used these predictions of wave displacement and velocity to modulate control forces. Forces opposing predicted Y_{mn} and V_{mn} increased the disk stiffness and damping, respectively.

Analysis of Spectral Controller Performance

The equations of motion of the disk are derived from Hamilton's Extended Principle [7].

$$\int_{t_1}^{t_2} \delta T^* - \delta V + \left[\int_A q \delta y dA \right] dt = 0 \quad (10)$$

where T^* is the disk kinetic coenergy (see Appendix), V is the potential energy and q are the external forces not derived from V . Admissible distributions y are of class C^1 satisfying the essential boundary conditions (order 0 and 1) and periodicity conditions;

$$\begin{aligned} y(a, \theta, t) &= y_r(a, \theta, t) = 0 \\ y(r, \theta, t) &= y(r, \theta + 2\pi, t) \\ y_r(r, \theta, t) &= y_{,\theta}(r, \theta + 2\pi, t) \end{aligned} \quad (11)$$

Discretization of the stationary value problem (10) is carried out using the Ritz Method with the $(M+1) \times (N+1)$ term admissible series

$$\begin{aligned} \hat{y}_{MN} &= \sum_{m=0}^M \sum_{n=0}^N [C_{mn}(t) \cos(n\theta) \\ &\quad + D_{mn}(t) \sin(n\theta)] R_{mn}(r) \end{aligned} \quad (12)$$

with generalized coordinates $C_{mn}(t)$, $D_{mn}(t)$, and $R_{mn}(r) = (r-a)^2 [1 + K_1(r/b) + K_2(r/b)^2]$. The constants, K_1 and K_2 , were calculated from a rotating disk analysis [8].

The transverse forces q in (10) were modeled as the rotating and stationary viscous forces in (13a) and (13b), respectively.

$$q_r = -c_r [y_{,t} + \Omega y_{,\theta}] \quad (13a)$$

$$q_s = -c_s [y_{,t}] \quad (13b)$$

The coupled discrete differential equations of motion obtained from (10)-(13) are

$$\begin{aligned} I_{mn} [\ddot{C}_{mn} + 2n\Omega \dot{D}_{mn} - n^2 \Omega^2 C_{mn}] \\ + [c_r + c_s] \dot{C}_{mn} + [L_{mn} + J_{mn}] C_{mn} \\ + [n\Omega c_r] D_{mn} - Q_{mn}^C = 0 \end{aligned} \quad (14a)$$

$$\begin{aligned} I_{mn} [\ddot{D}_{mn} - 2n\Omega \dot{C}_{mn} - n^2 \Omega^2 D_{mn}] \\ + [c_r + c_s] \dot{D}_{mn} + [-n\Omega c_r] C_{mn} \\ + [L_{mn} + J_{mn}] D_{mn} - Q_{mn}^D = 0 \end{aligned} \quad (14b)$$

where the Appendix gives I_{mn} , the inertia coefficients for $m=1, \dots, M$, $n=1, \dots, N$; L_{mn} , the bending stiffness coefficients; J_{mn} , the membrane stress stiffness coefficients; and Q_{mn}^C , and Q_{mn}^D , the external control forces. Forces rotating with the disk q_r , always dissipate energy independent of Ω . Stationary forces, q_s , interact with disk transverse velocity at their position. A critical disk rotation speed exists for each wave [4, 9] which exactly equals the wave propagation velocity as viewed in the stationary frame. At the Critical Speed, the characteristic frequency and transverse velocity of the wave are zero in the stationary reference frame and stationary dissipative forces cannot increase the dissipation of that wave. The separation of dissipative forces into moving and stationary components is an open topic.

Stability of the axisymmetric disk response is predicted

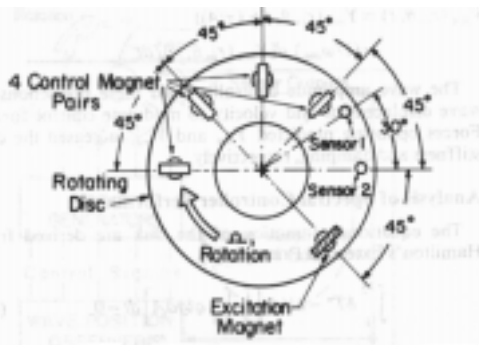


Fig. 3(a) Prototype controller sensor and magnet positions

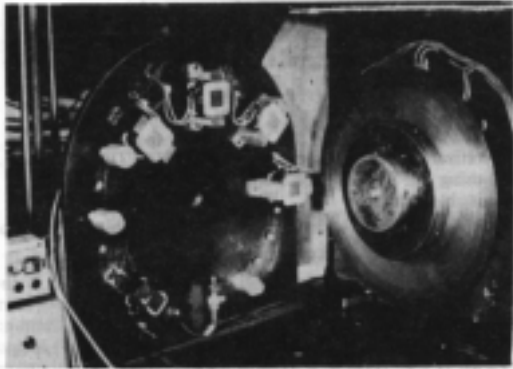


Fig. 3(b) Prototype spectral controller test stand showing sensor/magnet mount

Prototype spectral controller with sensor/magnet mount
 Above: controller sensor and magnet positions

from the eigenvalue problem derived from (14) and the control forces Q_{mn}^D and Q_{mn}^C . Here the control forces are proportional to the predicted Y_{mn} and V_{mn}

$$q = -K_p Y_{mn} - K_D V_{mn} \quad (15)$$

The eigenvalue problem obtained from the Laplace transform of (14) and (15) is

$$[s^2 M + sC + P + Q(s, \tau)] X(s) = Q \quad (16)$$

where M is the inertia matrix, C is the damping matrix, P is the disk stiffness matrix, $Q(s, \tau)$ is the control force matrix and $X^T(s)$ is the $[C^T, D^T]$. The eigenvalues s are roots of the characteristic equation

$$\det[s^2 M + sC + P + Q(s, \tau)] = 0 \quad (17)$$

The roots of (17) were found using Muller's Method [10].

Steady-state response of the controlled disk to constant amplitude harmonic excitation was calculated using the results of the eigenvalue analysis above. A modal mass for each generalized coordinate was calculated from the frequency response of an uncontrolled disk. These modal masses allowed conversion of controlled disk eigenvalues to predictions of mode response to external disturbance forces. The direct calculation of forced response for the controlled disk was avoided because of the complicated form of the control force terms in the disk equations of motion.

Laboratory Implementation and Testing

A prototype control system was constructed to evaluate its

potential performance. The test disk was uniform and circular with radii $b = 203$ mm and $a = 101.5$ mm and thickness $t = 1.02$ mm. The transverse displacements were measured with two Bentley-Nevada non-contacting inductive sensors, and active control forces were applied by energizing electro-magnets. The magnet units were constructed in opposing pairs, one on each disk surface. Two and four magnet pairs were tested as shown in Fig. 3. An independent excitation magnet simulated the transverse disturbances of the process. Two minicomputers (DEC PDP 8/E) performed the spectral observer and wave amplitude controller tasks.

The control system provided additional damping in all laboratory tests by developing forces opposing V_{mn} . The small structural damping of the steel disk tested could be significantly increased by control forces less than 10 Newtons. Control forces of this magnitude produced relatively small stiffness increases.

The steady-state response of the control system was measured for combinations of rotation speed, wave under control, and number of magnet pairs. Initially the rotating disk was excited with broad band random transverse forces and the spectral observer identified the waves with largest amplitude. Typically, the five waves with largest amplitude were identified. The spectral observer selected the wave for control, as discussed earlier. To simulate adverse vibration present in production sawing process and measure the effect of the control on vibration dominated by the response of a single wave, the excitation was then changed to a constant amplitude harmonic force at the characteristic frequency of the wave, the control system was energized, and the gain of the controller increased incrementally while disk response was monitored.

Results

An eigenvalue analysis (16) for a rotating disk under two distributed control forces is shown in Fig. 4. The disk stationary damping ratio was $\zeta_s = 0.005$ and the rotating damping was zero in the analyses. The control force distributions were separated by 45 degrees. Each was centered at $r = 160$ mm and had an area of 294 sq mm.

As the control gain is increased from 0 to 1250 Newtons/meter, the real part of the controlled wave eigenvalue becomes increasingly negative. Most eigenvalues are independent of the control. However, in this example the one nodal diameter, zero nodal circle eigenvalue is shifted in a positive, destabilizing direction and establishes the stability gain limit for the control system. The destabilizing behavior results from the comb filter algorithm, which passes all harmonics of the recirculation frequency. In Fig. 4 the wave $(m, n) = (0, 1)$ is at the first harmonic of the recirculation frequency, and it destabilizes the control. This example illustrates an inherent problem in the control of systems that are rich in waves with low damping. It is likely that some frequency will reside at an integer multiple of the control frequency and it will be energized by the control because of the force-response phase. The digital filter used here was chosen for its simplicity and to demonstrate this type of instability. Other digital filters can be designed which will increase the maximum stable control gain, however, this instability associated with aliasing will always occur at some gain for all filters.

Analysis of four control forces in Table 1 shows a proportional increase in damping at the gain limit for stability. The improved controller effectiveness resulted from orthogonality between the control force distribution and the non-controlled wave eigenfunctions. The eigenvalue analysis showed the spectral controller would increase damping of the controlled waves resulting in a decrease in the steady-state forced response.

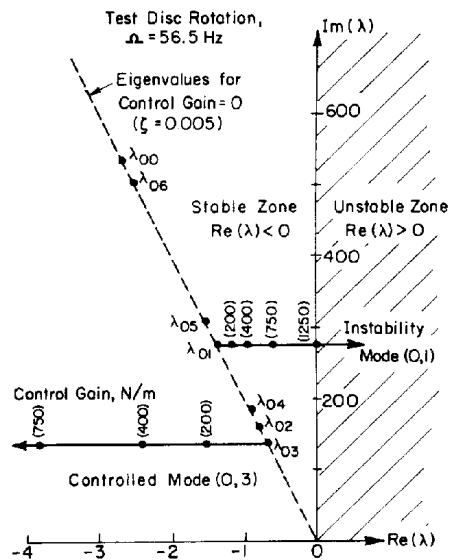


Fig. 4 Typical eigenvalue analysis results

Laboratory test results in Table 2 and Figs. 5-7 show the decrease in transverse amplitude response with increasing control gain. The wave response is X/F_e where X is the measured average controlled wave amplitude under the two sensors, and F_e is the excitation force amplitude. The control gain, G , is the ratio of control force amplitude at each control magnet position to X . The data points in Figs. 5-7 result from laboratory measurements and the solid curves are derived independently from the analysis using measurements of uncontrolled disk damping. The wave response at each G decreased in proportion to the number of control forces because total dissipation was proportional to the product of control force amplitude and the number of control forces applied. The wave amplitude is inversely proportional to damping which was proportional to G . The principal benefit of the control was obtained at small control gains.

The comb filter harmonic instability predicted analytically in Fig. 4 occurred in one of the laboratory tests. Controller test C in Table 2 and Fig. 7, was configured to encourage harmonic instability. Harmonic instability in the (0, 1) wave limited the minimum (0, 3) wave response to $X/F_e = 0.058$ mm/N with two control forces and $X/F_e = 0.037$ mm/N with four control forces. This increase in control from additional control forces was similar to that predicted by analysis. Additional instability observed with the prototype system was attributed to inability of the wave observer to track rapid changes in mode characteristic frequency resulting from control.

Transient response of the control system was observed under abruptly terminated external excitation. At small G , the controlled wave amplitude decayed in proportion to G . At large G , a limiting decay rate was observed. This behavior is determined by the response speed of the comb filter. The roots of the comb filter transfer function determine a decay rate equivalent to a 2.1 percent damping ratio. Transient decay of wave amplitude is limited to this value and a detailed analysis is given in [11]. Filter designs with faster response would be desirable.

Conclusion

Spectral analysis has been shown to be an effective means

of identifying modes represented by travelling waves on a rotating disk. In laboratory tests with a steel disk, characteristic frequencies were identified from local maxima in the Fast Fourier Transforms of two transverse displacement signals. At these maxima, the corresponding wave shapes were identified from the phase relationship between the two signals. In experiments four to six waves with largest amplitudes were reliably identified.

The system successfully tracked individual travelling waves in experiments on rotating disks. Transverse control forces, developed to increase damping, resulted in reductions in response amplitudes between 84 and 93 percent of the uncontrolled amplitude.

Instabilities in the controller were of two types and both were attributed to the comb filter behavior. First, harmonics of the filter center frequency are passed thereby distorting the wave estimation. Second, instability is associated with inability of the filter to rapidly track changes in characteristic frequency. Digital filter algorithms and frequency tracking methods bypassing the limitations would be of significant value.

The laboratory tests demonstrated that significant vibration reduction can be achieved before the onset of instability. Wave response reductions of 75 percent were achieved in every test through increased damping from low frequency control forces. Because relatively small additional benefit is obtained at higher control gains, these stable levels of control are reasonable expectations for single waves. Increased vibration control can be realized through the control of many waves. The extension of the spectral control algorithm to the control of multiple waves only requires superposition of wave amplitude controller outputs. The analytical predictions and the laboratory observations of wave amplitude were within 10 percent of for stable operating gains. Observed instabilities of the control system are also predicted by the analysis.

Implementation of the control method should be accomplished with dedicated circuitry. Digital filters and Fast Fourier Transform technology are at the integrated circuit "chip" state. The post-FFT analysis is well suited to the parallel processing microprocessors currently under development.

The disk motion was dominated by low frequency waves so only low frequency control forces were required. The types of force generators which can be used by this control method are many. For example, fluid pressure differential can be used to control vibration in these systems.

Acknowledgments

The authors are grateful for the generous financial support provided by the following companies and agencies: University of California Forest Products Laboratory, California Cedar Products Co., California Saw and Knife Inc., CIRIS, Hudson Lumber Co., McMillan Bloedel Research Ltd., the National Science Foundation, Potlatch Corp., Simpson Timber Co., Stimson Lumber Co./Miller Redwood Co., Sun Studs Inc., and the Weyerhaeuser Co.

References

- 1 Mote, C. D., Jr., and Holgyen, S., "Confirmation of the Critical Speed Theory for Symmetrical Circular Saws," *ASME Journal of Engineering for Industry*, Vol. 97, No. 3, 1975, pp. 1112-1118.
- 2 Ellis, R. W., and Mote, C. D., Jr., "A Feedback Vibration Controller for Circular Saws," *ASME JOURNAL OF DYNAMIC SYSTEMS, MEASUREMENT, AND CONTROL*, Vol. 101, Mar. 79, pp. 44-49.
- 3 Balas, M. J., "Feedback Control of Flexible Systems," *IEEE Trans. on Automatic Control*, Vol. ac-23, No. 4, 1978, pp. 673-679.
- 4 Mote, C. D., Jr., "Stability of Circular Plates Subjected To Moving Loads," *J. Franklin Inst.*, Vol. 290, No. 4, Oct. 1970, pp. 329-344.
- 5 Tobias and Arnold, "The Influence of Dynamical Imperfections on the Vibration of Rotating Discs," *Proc. Institute of Mechanical Engineering*, Vol. 171, 1937, pp. 669-690.

Table 1 Eigenvalue analysis of increased damping from spectral control

Rotation Freq. Ω (Hz)	Controlled Mode m,n	Wave Nat. Freq. ω_{mn}^* (Hz)	Damping Ratio ζ	$\frac{\zeta_{con}}{\zeta_{un}}$	Instability Mode m,n	Analysis Case
56.5	0,3	22.0	0.005	-----	-----	No Control
56.5	0,3	22.0	0.042	8.4	0,1	2 Control Forces
56.5	0,3	22.0	0.073	14.8	0,1	4 Control Forces

Table 2 Laboratory test conditions for results shown in Figs. 5-7

Series Identifier	Control Forces	Disc Rotation Speed, Hz.	Controlled Wave: m,n	Wave Natural Freq.: ω_{mn}^*
A-4	4	55.0	0,2	23.6
A-2	2	55.0	0,2	23.6
B-4	4	55.0	0,3	19.4
B-2	2	55.0	0,3	18.8
C-4	4	58.1	0,3	14.3
C-2	2	58.1	0,3	14.2

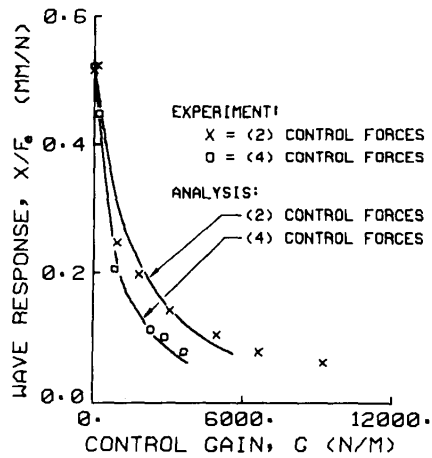


Fig. 5 Results of experiment and analysis for control test A

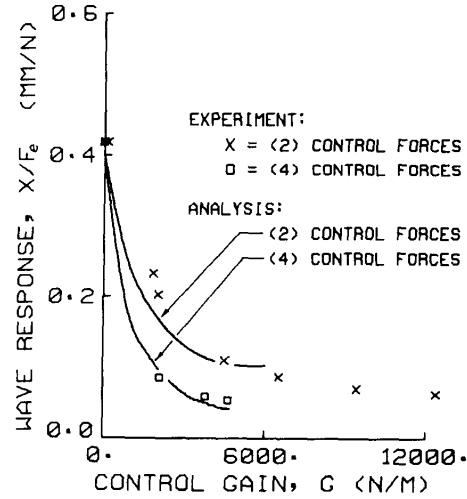


Fig. 6 Results of experiment and analysis for control test B

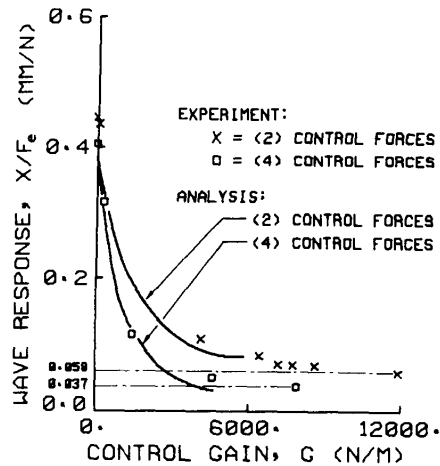


Fig. 7 Results of experiment and analysis for control test C

6 Rader, C. M., and Gold, B., "Digital Filter Design Techniques In The Frequency Domain," *Proc. IEEE*, Vol. 55, Feb. 1967, pp. 149-171.
 7 Rayleigh, J. W. S., *Theory of Sound*, Dover Press, New York, 1945, pp. 353-371.
 8 Schajer, G. S., "Optimizing Saw Design and Operation: Circular Saw Natural Frequency Program SAWFQ2," Tech. Rep. No. 35.01.130, Progress Rep. No. 13, Univ. of Calif. Forest Products Lab., Richmond, Calif., 1979.
 9 Southwell, R. V., "On the Free Transverse Vibration of a Uniform Circular Disc Clamped at its Centre: and on the Effects of Rotation," *Proceedings, Royal Society of London, Series A*, Vol. 101, 1921, pp. 133-153.
 10 Conte, S. D., and Deboor, C., *Elementary Numerical Analysis: An Algorithmic Approach*, McGraw-Hill, 2nd Ed., 1972, pp. 74-83.
 11 Radcliffe, C. J., *Active Control of Vibration in Rotating Circular Discs*, Ph.D. dissertation, University of California, Berkeley, June 1980.

APPENDIX

The kinetic coenergy, T^* , and potential energy, V , in Hamilton's Extended Principle (10) for a rotating disk are presented below.

$$\begin{aligned}
 T^* &= \iint_A (\rho h/2)(Dy/Dt)^2 dA \\
 &= \iint_A (\rho h/2)(y_{,t} + \Omega y_{,\theta})^2 dA \\
 V &= \iint_A (D/2)[(\nabla^2 y)^2] dA \\
 &\quad - \iint_A D(1-\nu)[y_{,rr}(y_{,r}/r + y_{,\theta\theta}/r^2) \\
 &\quad\quad - (y_{,\theta}/r)_{,r}] dA \\
 &\quad + \iint_A (h/2)[\sigma_r(y_{,r}) + \sigma_\theta(y_{,\theta}/r)^2 \\
 &\quad\quad + 2\tau_{r\theta}y_{,r}(y_{,\theta}/r)] dA \\
 &\quad + \iint_A (h/2E)[(\sigma_r + \sigma_\theta)^2 - 2(1-\nu)(\sigma_r\sigma_\theta - \tau_{r\theta}^2)] dA \quad (A2)
 \end{aligned}$$

where:

$D = Eh^3/[12(1-\nu^2)]$ = disk plate rigidity
 h = disk thickness
 ρ = disk density
 σ_r = radial stress
 σ_θ = hoop stress
 $\tau_{r\theta}$ = shear stress
 $y_{,t} = \partial y/\partial t$, $y_{,\theta} = \partial y/\partial \theta$, etc.

The parameters in the equations of motion for the rotating disk (14) result directly from application of the Ritz Method

on a variational problem derived from Hamilton's Extended Principle [1, 5]. They are given below.

$$\begin{aligned}
 (A1) \quad I_{mn} &= \int_a^b \rho h R_{mn}^2 r dr \\
 L_{mn} &= (L_{mn}^{22} + 2L_{mn}^{12} - 2n^2 L_{mn}^{02} + L_{mn}^{11} - 2n^2 L_{mn}^{01} + n^4 L_{mn}^{00}) \\
 &\quad - 2(1-\nu)(L_{mn}^{12} - n^2 L_{mn}^{02} - n^2 L_{mn}^{11} + 2n^2 L_{mn}^{01} - n^2 L_{mn}^{00}) \\
 L_{mn}^{00} &= \int_a^b D(R_{mn}/r^2)^2 r dr \\
 L_{mn}^{01} &= \int_a^b D(R_{mn}/r^2)(R'_{mn}/r) r dr \\
 L_{mn}^{02} &= \int_a^b D(R_{mn}/r^2)R''_{mn} r dr, L_{mn}^{11} = \int_a^b D(R'_{mn}/r)^2 r dr \\
 L_{mn}^{12} &= \int_a^b D(R'_{mn}/r)R''_{mn} r dr, L_{mn}^{22} = \int_a^b D(R''_{mn})^2 r dr \\
 J_{mn} &= \int_a^b (h\sigma_r R_{mn}'^2 + n^2 h\sigma_\theta R_{mn}^2/r^2) r dr
 \end{aligned}$$

$$Q_{mn}^A = (1/\pi) \iint_A q(r, \theta, t) \cos(n\theta) R_{mn} dA, \text{ control force term}$$

$$Q_{mn}^B = (1/\pi) \iint_A q(r, \theta, t) \sin(n\theta) R_{mn} dA, \text{ control force term}$$

where: $c_{mn} = 2\sqrt{J_{mn}(L_{mn} + J_{mn})}$, for convenience and prime (') denotes spacial derivative (i.e., $\partial/\partial r$)